Entanglement-enhanced detection of single-photon scattering

C. Hempel[1,2], B. P. Lanyon[1], P. Jurcevic[1,2], R. Gerritsma[1†], R. Blatt[1,2], C. F. Roos[1,2*]
[1] *Institut für Quantenoptik und Quanteninformation, Österreichische Akademie der Wissenschaften, Technikerstr. 21a, 6020 Innsbruck, Austria*
[2] *Institut für Experimentalphysik, Universität Innsbruck, Technikerstr. 25, 6020 Innsbruck, Austria*
(Dated: January 16, 2013)

arXiv:1304.3270v1 [quant-ph] 11 Apr 2013

The ability to detect the interaction of light and matter at the single-particle level is becoming increasingly important for many areas of science and technology. The absorption or emission of a photon on a narrow transition of a trapped ion can be detected with near unit probability [1, 2], thereby enabling ultra-precise ion clocks [3, 4] and quantum information processing applications [5]. Extending this sensitivity to broad transitions is challenging due to the difficulty of detecting the rapid photon scattering events in this case. Here we demonstrate a technique that enables the scattering of a single photon on a broad optical transition to be detected with high probability. Our approach is to use an entangled state to amplify the tiny momentum kick an ion receives upon scattering a photon. The method should find applications in spectroscopy and quantum information processing.

An ion in an electric trap provides an excellent system for carrying out precision spectroscopy. Laser cooling [6], either directly or sympathetically via an auxiliary ion [7], minimises thermal line broadening. Long storage times allow for many repeated measurements on the same particle and collisional shifts are non-existent. A key requirement is to detect whether photons of a given frequency are scattered. For some narrow ionic transitions, corresponding to long excited-state lifetimes, the electronic configuration change associated with photon absorption or emission can be detected with near 100% efficiency using the electron shelving technique [1]. In the general case where electron shelving cannot be implemented directly on a 'spectroscopy' ion of interest, efficient detection is possible using a co-trapped auxiliary 'logic' ion following the technique of quantum logic spectroscopy [8]. Here, information about the electronic state of the spectroscopy ion is mapped via a joint vibrational mode to the electronic state of the logic ion, where it can be read out. For broad transitions, quantum logic spectroscopy fails due to the extremely short excited state lifetimes and resulting inability to spectrally resolve their vibrational sidebands [2].

Another signature of a photon scattering event is the recoil kick an ion receives upon absorbing or emitting a photon [9]. The size of the recoil can be characterised by the ratio of the recoil energy $E_{\rm rec}$ to the energy of a quantum of motion $h\nu$ of an harmonically trapped ion oscillating at frequency ν in the form of the Lamb-Dicke factor $\eta{=}\sqrt{E_{\rm rec}/(h\nu)}$, which typically fulfils $\eta{\ll}1$ in experiments on optical transitions. For an ion cooled to its motional ground state, the probability of being promoted to the next higher vibrationally excited state by the recoil of an absorbed photon is η^2. Consequently, the method of monitoring the ground-state population is inefficient for detecting absorption events. Spectral lines from broad transitions have been reconstructed by observing changes in the fluorescence of a laser-cooled control ion via scattering of many 100's of photons [10] or via an off-resonantly induced optical dipole force [11].

We now describe a technique for amplifying the recoil signal of single photons, which is independent of the particular ion species employed (Fig. 1). As with quantum logic spectroscopy, a co-trapped logic ion encodes a two-level qubit with ground and excited states $|{\downarrow}\rangle_z$ and $|{\uparrow}\rangle_z$, respectively. The logic qubit and a common vibrational mode of the two-ion crystal are prepared in their respective ground states. A state-dependent force applied to this mode splits the vibrational state into two parts, each correlated with a different eigenstate in the logic qubit [12, 13]. Consequently, logic qubit and motional state become entangled into a Schrödinger cat state of the form $\Psi{=}(|{\rightarrow}\rangle_x|{+}\alpha\rangle + |{\leftarrow}\rangle_x|{-}\alpha\rangle)/\sqrt{2}$, where $|{\rightarrow}\rangle_x$ and $|{\leftarrow}\rangle_x$ are eigenstates of the σ_x Pauli operator and $|\pm\alpha\rangle$ are coherently displaced motional states.

In the next step, spectroscopy light is sent in at a known frequency. The inverse cat generation operation is then applied, thereby recombining the two vibrational components of the cat state and disentangling them from the logic qubit. If no spectroscopy photon was absorbed, the initial state of the logic qubit $|{\downarrow}\rangle_z$ is recovered. Otherwise, the recoil of the spectroscopy ion causes both vibrational components to be displaced by $\eta_{\rm abs}$ so that after recombination the total path encloses an area in phase space. The result is a geometric phase [14] $\phi_{\rm abs}{=}2\alpha\eta_{\rm abs}\sin(\phi_{\rm tr})$ proportional to the cat state size α, which leaves the final logic qubit state rotated by $\exp(i\phi_{\rm abs}\sigma_x)$ [15, 16]. Here, $\phi_{\rm tr}{=}2\pi\nu\tau$ where τ is the time delay between photon absorption and the time of largest spatial extent of Ψ oscillating at frequency ν. Measurements of the logic qubit spin projections $\langle\sigma_z\rangle{=}{-}\cos(\phi_{\rm abs})$ or $\langle\sigma_y\rangle{=}\sin(\phi_{\rm abs})$, using standard electron shelving for example, provide information about

†present address: QUANTUM, Institut für Physik, Universität Mainz, Staudingerweg 7, 55128 Mainz, Germany
*corresponding author (christian.roos@oeaw.ac.at)

the photon absorption process. In summary, the small recoil displacement of the spectroscopy ion is converted into a large geometric phase and mapped onto the logic qubit's electronic state.

A complete photon scattering event involves two momentum kicks – one in absorption and one in emission. Since the absorbed photon comes from a directed laser beam, ideally this beam points parallel to the vibrational mode supporting the cat state. The recoil direction due to the spontaneously emitted photon is random. The effect is to add a second, random geometric phase $\phi_{\rm em}$ to the measured signal: $\langle\sigma_z\rangle = -\overline{\cos(\phi_{\rm abs}+\phi_{\rm em})}$, where the bar indicates averaging with respect to $\phi_{\rm em}$. For an isotropic emission pattern, this expression reduces to

$$\begin{aligned}\langle\sigma_z\rangle &= -\cos(\phi_{\rm abs})\,{\rm sinc}(\phi_{\rm em}) \\ &= -\cos(2\alpha\eta_{\rm abs}\sin\phi_{\rm tr})\,{\rm sinc}(2\alpha\eta_{\rm em}\sin\phi_{\rm tr}), \quad (1)\end{aligned}$$

and similarly $\langle\sigma_y\rangle = \sin(\phi_{\rm abs})\,{\rm sinc}(\phi_{\rm em})$.

In our demonstration we confine a mixed-species two-ion crystal in a linear Paul trap (see Methods). The isotopes $^{40}Ca^+$ and $^{44}Ca^+$ are employed as logic and spectroscopy ion, respectively (Fig. 2a). The $^{40}Ca^+$ provides sympathetic Doppler and vibrational ground state cooling of the lowest frequency axial vibrational mode at $\nu = 1.199$ MHz, a long-lived electronic transition in which to encode a qubit ($S_{1/2} \rightarrow D_{5/2}$) and qubit state readout via electron shelving. Spectroscopy is performed on the strong $D_{3/2} \rightarrow P_{1/2}$ open dipole transition in $^{44}Ca^+$, which has an excited state lifetime of 7.1 ns [17] and, with 93.5% probability, will absorb only one photon before spontaneously decaying to the $S_{1/2}$ ground state [18].

The experimental sequence is presented in Fig. 2b. A state-dependent force [19] is realised using a bichromatic laser field resonant with the red ($-\nu$) and blue ($+\nu$) vibrational sidebands of the logic qubit. Precise timing of the absorbed photon with respect to the phase of Ψ oscillating at ν is achieved using a phase-coherent train of spectroscopy pulses, each of $\sim$60 ns duration and separated by $1/\nu$. Scanning the time delay τ between the cat-state oscillation and the pulse train gives rise to interference fringes (Fig. 3a). Since the signal $\langle\sigma_z\rangle$ (blue curve) is insensitive to the sign of the geometric phase shift, the fringe period is equal to half the motional period. Conversely, the signal $\langle\sigma_y\rangle$ (red curve) is sign sensitive and therefore oscillates around 0 with a period equal to the motional period $1/\nu$. Furthermore, while the signal in $\langle\sigma_z\rangle$ is sensitive to the recoils of absorbed and reemitted photon, the signal in $\langle\sigma_y\rangle$ is predominantly due to the recoil of the absorbed photon (the reemitted photon causes just a slight loss of contrast). The signal in $\langle\sigma_y\rangle$ is therefore, with high probability, due to a single photon absorption event.

A line profile of the single-photon transition in $^{44}Ca^+$ was recovered using the cat state technique (Fig. 3b). The $\langle\sigma_y\rangle$-signal amplitude was measured as a function of the spectroscopy laser frequency at a reduced light intensity. The observed line-width of 38(5) MHz is close to the width expected due to the combination of the transition's natural linewidth (22.4 MHz) with the Zeeman splitting caused by an applied magnetic field of 4 Gauss. We wish to emphasise that this profile is due, with high probability, to only a single infrared photon scattering on an open dipole transition.

The uncertainty in the spectroscopic signal is determined by quantum projection noise [20] in estimating the expectation values of the logic qubit state. The signal-to-noise ratio (SNR) can always be increased by taking more measurements. To compare different methods it is therefore useful to renormalise by the number of measurements N made and consider the sensitivity $\beta = SNR/\sqrt{N}$ provided by each method. For comparison we implemented two additional direct detection schemes that do not exploit a non-classical state to amplify the scattering signal. The first and most basic of the two schemes directly measures the probability of the motional state being excited from $|0\rangle$ to $|1\rangle$ (phonons) by a single photon scattering event by applying a red-sideband π pulse to the logic ion followed by a measurement of $\langle\sigma_z\rangle$. In the second scheme, $\langle\sigma_y\rangle$ is measured instead and phase sensitive detection of the motional state is enabled by keeping the pulse envelope of the spectroscopy laser phase-locked to the beat signal (at frequency ν) of the two laser fields manipulating the ions' motion.

Table I summarises the experimentally determined sensitivities. Compared to the direct detection method, cat-state spectroscopy enabled an 18-fold improvement in measurement sensitivity. Also presented are results showing that unlike the direct detection methods, cat-state spectroscopy even works *without* ground state cooling. Theoretically, the method should work as well with thermal states that lie within the Lamb-Dicke regime, which can be reached with standard Doppler cooling [21]. Experimentally, a loss in contrast is seen whose origin requires additional study.

In principle, the technique's sensitivity can be further enhanced by making larger cat states. However, experimental errors will limit the useful cat size and thereby the obtainable sensitivity. In our experiment the dominant error source is electric field noise on the trap electrodes, which adds another random geometric phase $\phi_{\rm h}$. As a result, the contrast of the signal given in equation (1) needs to be multiplied by a factor $\exp(-\overline{\phi_{\rm h}^2}/2)$ with $\overline{\phi_{\rm h}^2} = 8R_{\rm h}n_{\rm cat}(\frac{2}{3}\tau_{\rm cat} + \tau_{\rm wait})$ where $R_{\rm h}$ is the mode's heating rate, $n_{\rm cat} = |\alpha|^2$ the cat state size in phonons, $\tau_{\rm cat}$ the time needed for creating the cat state and $\tau_{\rm wait}$ the time between cat creation and recombination. The larger the cat state, the more detrimental the noise becomes. For the $\langle\sigma_y\rangle$ measurement in Fig. 3a and the experimental parameters $n_{\rm cat} = 8.3(1.0)$, $\tau_{\rm cat} = 50(2)\,\mu$s, $\tau_{\rm wait} = 32\,\mu$s, $R_{\rm h} = 40(20)$ s^{-1}, we expect a contrast reduction factor of 0.91(5) and an overall signal amplitude of $A_{\rm y} = 0.54(4)$, which is close to the observed value.

We have demonstrated a method for detecting light scattering from broad ionic transitions at the single-photon level. Complementing quantum logic spec-

troscopy for narrow transitions, cat state spectroscopy should provide access to a new range of atomic and molecular ion transitions for precision spectroscopy. The achieved sensitivity could be boosted even further by using a larger ion trap to provide a reduced electric field noise, or better electronic filtering. Assuming that the absorbed and emitted photons have the same wavelength, equation (1) gives the maximum probability of detecting a scattering event, in a single measurement, as 61%. The limit, imposed by the random emission direction of the emitted photon, could be overcome by modifying the emission direction, e.g. by employing additional laser pulses to stimulate emission, the introduction of a cavity or by using phased arrays of multiple spectroscopy ions. A *deterministic* measurement of whether an ion has scattered a photon would be of interest to the field of quantum information processing, especially since this measurement could be non-destructive with respect to the joint ion-photon state. This desired aspect is addressed by recent theoretical proposal by Mur-Petit et al. [22].

Methods

Experimental setup. Experiments employ a linear Paul trap with a minimal ion-electrode distance of 565 µm. Ions are loaded by isotope-selective photoionization from a resistively heated oven. The bichromatic laser beam used to create and reinterfere the cat state is generated by applying two radio frequencies offset by 2ν to a single acousto-optic modulator, effectively producing a beat-note to which the generator producing the pulse-train of spectroscopy light is locked.

Geometric phases contributing to the spectroscopic signal. The total geometric phase that rotates the logic qubit state is given by $\phi{=}\phi_{\rm abs}+\phi_{\rm em}+\phi_{\rm h}$ resulting from photon absorption and emission recoil, and random electric fields displacing the ions, respectively. The magnitude of the phase $\phi_{\rm abs}{=}2\alpha\eta_{\rm abs}\sin\phi_{\rm tr}$ is the same in every experimental run and is determined by the cat state size α and the timing of the photon scattering event described by $\phi_{\rm tr}$. The other two phases are independent random variables with vanishing odd-order moments. This property simplifies the calculation of expectation values at the end of the spectroscopy protocol, leading to $\langle\sigma_z\rangle{=}\ -\ \overline{\cos(\phi_{\rm abs}+\phi_{\rm em}+\phi_h)}{=}\cos(\phi_{\rm abs})\overline{\cos\phi}_{\rm em}\,\overline{\cos\phi_{\rm h}}$ and $\langle\sigma_y\rangle{=}\overline{\sin(\phi_{\rm abs}+\phi_{\rm em}+\phi_h)}{=}\sin(\phi_{\rm abs})\overline{\cos\phi}_{\rm em}\,\overline{\cos\phi_{\rm h}}$. The recoil in spontaneous emission creates the phase $\phi_{\rm em}{=}2\alpha\eta_{\rm em}\sin\phi_{\rm tr}\cos\theta\ \equiv\ \tilde{\phi}_{\rm em}\cos\theta$, where θ describes the angle between the directions of photon emission and normal mode oscillation. As spontaneous emission from the $P_{1/2}$ to $S_{1/2}$ state is isotropic, $\overline{\cos\phi}_{\rm em}{=}\frac{1}{2}\int_0^\pi d\theta\sin\theta\,\cos(\tilde{\phi}_{\rm em}\cos\theta)$. Carrying out the integration results in the sinc-function appearing in equation (1).

Electric field noise at the trap electrodes with frequencies close to the vibrational mode supporting the cat state leads to displacements of the motional state in random directions. White noise acting on a cat of size $n_{\rm cat}$ for a duration τ adds a random geometric phase $\phi_{\rm h}$ with zero mean and a variance given by $\overline{\phi_{\rm h}^2}{=}8R_{\rm h}n_{\rm cat}\tau$ [15]. In our model, we assume noise acting on the state throughout the experimental steps of cat state creation, photon scattering and cat recombination, the steps lasting times $\tau_{\rm cat}$, $\tau_{\rm wait}$ and $\tau_{\rm cat}$, respectively. If a spin-dependent force of constant amplitude is used for cat creation and recombination, we have to make the replacement $\tau\rightarrow\frac{1}{3}2\tau_{\rm cat}+\tau_{\rm wait}$ where the factor $\frac{1}{3}$ accounts for the smaller average cat size during the first and last steps (see Supplementary Information).

[1] Dehmelt, H. G. Mono-ion oscillator as potential ultimate laser frequency standard. *IEEE T. Instrum. Meas.* **31**, 83–87 (1982).

[2] Leibfried, D., Blatt, R., Monroe, C. & Wineland, D. Quantum dynamics of single trapped ions. *Rev. Mod. Phys.* **75**, 281–324 (2003).

[3] Rosenband, T. *et al.* Frequency ratio of al^+ and hg^+ single-ion optical clocks; Metrology at the 17th decimal place. *Science* **319**, 1808–1812 (2008).

[4] Chou, C., Hume, D., Koelemeij, J., Wineland, D. & Rosenband, T. Frequency comparison of two high-accuracy al^+ optical clocks. *Phys. Rev. Lett.* **104**, 070802 (2010).

[5] Häffner, H., Roos, C. F. & Blatt, R. Quantum computing with trapped ions. *Phys. Rep.* **469**, 155–203 (2008).

[6] Wineland, D. & Itano, W. Laser cooling of atoms. *Phys. Rev. A* **20**, 1521–1540 (1979).

[7] Larson, D., Bergquist, J., Bollinger, J., Itano, W. & Wineland, D. Sympathetic cooling of trapped ions: A laser-cooled two-species nonneutral ion plasma. *Phys. Rev. Lett.* **57**, 70–73 (1986).

[8] Schmidt, P. O. *et al.* Spectroscopy using quantum logic. *Science* **309**, 749–752 (2005).

[9] Weiss, D. S., Young, B. C. & Chu, S. Precision measurement of the photon recoil of an atom using atomic interferometry. *Phys. Rev. Lett.* **70**, 2706–2709 (1993).

[10] Clark, C. R., Goeders, J. E., Dodia, Y. K., Viteri, C. R. & Brown, K. R. Detection of single-ion spectra by Coulomb-crystal heating. *Phys. Rev. A* **81**, 043428 (2010).

[11] Hume, D. B. *et al.* Trapped-ion state detection through coherent motion. *Phys. Rev. Lett.* **107**, 243902 (2011).

[12] Poyatos, J., Cirac, J., Blatt, R. & Zoller, P. Trapped ions in the strong-excitation regime: Ion interferometry and nonclassical states. *Phys. Rev. A* **54**, 1532–1540 (1996).

[13] Monroe, C. R., Meekhof, D. M., King, B. E. & Wineland, D. J. A "Schrodinger cat" superposition state of an atom. *Science* **272**, 1131–1136 (1996).

[14] Chaturvedi, S., Sriram, M. S. & Srinivasan, V. Berry's phase for coherent states. *J. Phys. A: Math. Gen.* **20**, L1071–L1075 (1987).

[15] Turchette, Q. A. *et al.* Decoherence and decay of motional quantum states of a trapped atom coupled to engineered reservoirs. *Phys. Rev. A* **62**, 053807 (2000).

[16] Munro, W. J., Nemoto, K., Milburn, G. J. & Braunstein, S. L. Weak-force detection with superposed coherent states. *Phys. Rev. A* **66**, 023819 (2002).

[17] Jin, J. & Church, D. A. Precision lifetimes for the Ca^+ 4p ^{2}P levels: Experiment challenges theory at the 1% level. *Phys. Rev. Lett.* **70**, 3213–3216 (1993).

[18] Safronova, M. S. & Safronova, U. I. Blackbody radiation shift, multipole polarizabilities, oscillator strengths, lifetimes, hyperfine constants, and excitation energies in Ca^+. *Phys. Rev. A* **83**, 012503 (2011).

[19] Haljan, P. C., Brickman, K.-A., Deslauriers, L., Lee, P. J. & Monroe, C. Spin-dependent forces on trapped ions for phase-stable quantum gates and entangled states of spin and motion. *Phys. Rev. Lett.* **94**, 153602 (2005).

[20] Itano, W. *et al.* Quantum projection noise: Population fluctuations in two-level systems. *Phys. Rev. A* **47**, 3554–3570 (1993).

[21] Kirchmair, G. *et al.* Deterministic entanglement of ions in thermal states of motion. *New J. Phys.* **11**, 023002 (2009).

[22] Mur-Petit, J. *et al.* Temperature-independent quantum logic for molecular spectroscopy. *Phys. Rev. A* **85**, 022308 (2012).

[23] Lucas, D. *et al.* Isotope-selective photoionization for calcium ion trapping. *Phys. Rev. A* **69** (2004).

Acknowledgments

This work was supported by the European Commission via the integrated project AQUTE and a Marie Curie International Incoming Fellowship.

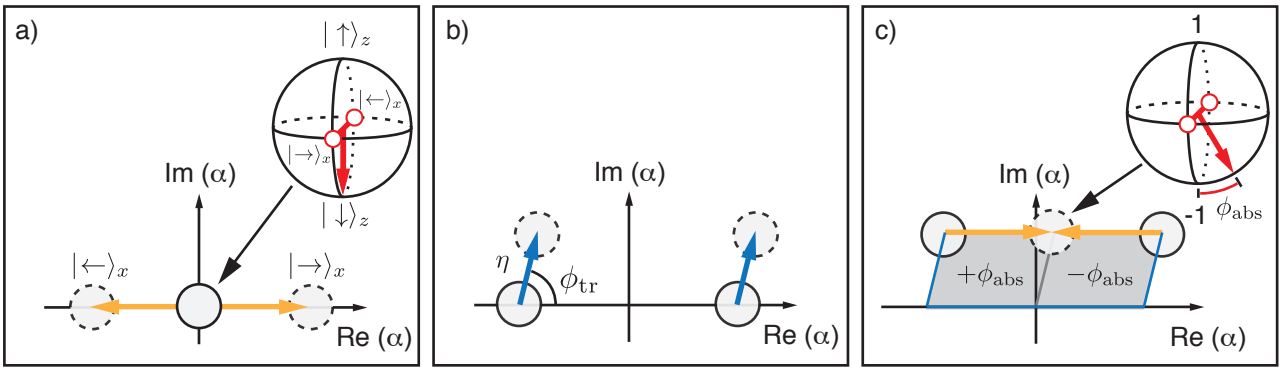

FIG. 1: **Cat state spectroscopy in phase space. a)** Schrödinger cat state preparation. A qubit encoded in a logic ion, initialized in $|\downarrow\rangle_z$ (inset Bloch sphere), becomes entangled with a joint vibrational mode of the two-ion crystal formed with the co-trapped spectroscopy ion. **b)** Absorption of a photon by the spectroscopy ion causes a displacement of size $\eta_{\rm abs}$ (magnified for clarity) in a direction determined by the event's timing relative to the cat-state's oscillation. **c)** The cat-state is reinterfered, disentangling the internal state from the motion and leaving the geometric phase $\phi_{\rm abs}$ in the logic ion's internal state, where it can be read out via standard electron shelving.

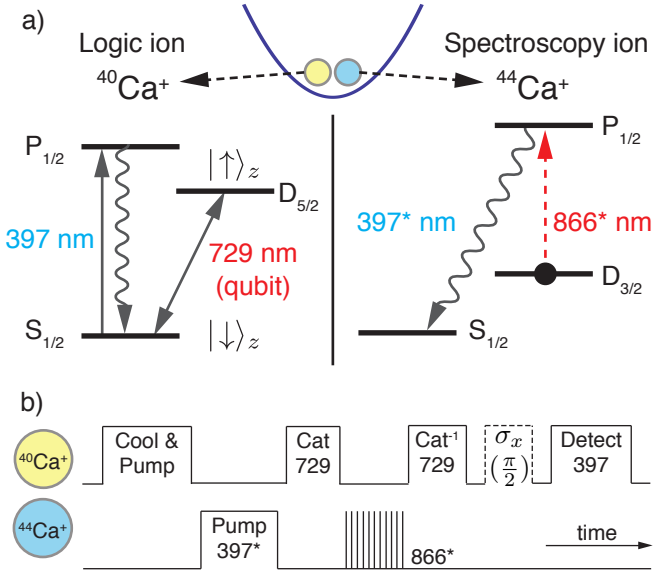

FIG. 2: **Experimental details. a)** Relevant electronic energy levels. **b)** Experimental laser pulse sequence. The $^{40}Ca^+$ dipole transition at 397 nm is used for laser cooling, optical pumping and state detection of the optical qubit implemented on its 729 nm narrow quadrupole transition, which is also used for ground state cooling of the joint vibrational mode. The * indicates isotope shifts [23] that allow off-resonant scattering from the respective other isotope to be safely ignored at the light intensities employed. Dedicated laser beams resonant with the $^{44}Ca^+$ transitions are used for initialization (397* nm) and spectroscopy (866* nm pulse train).

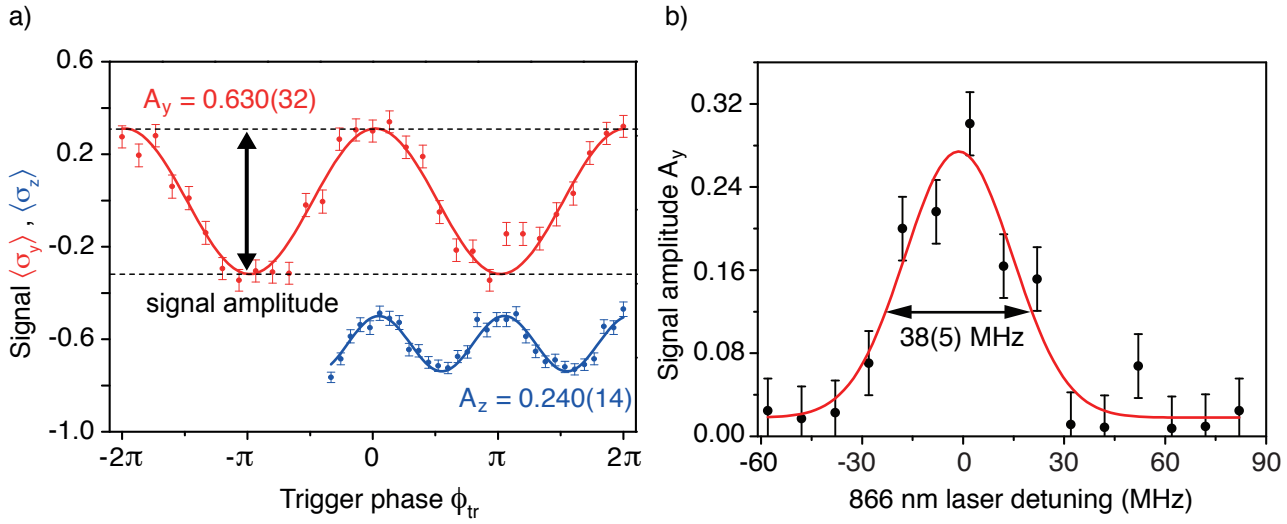

FIG. 3: **Cat state spectroscopy results.** Single photon scattering signals on the broad $D_{3/2} \rightarrow P_{1/2}$ transition in $^{44}Ca^{+}$. **a)** Interferometeric fringes observed by varying the phase difference $\phi_{\rm tr}$ between the spectroscopy pulse train and the cat state oscillation phase (see text). Weighted sinusoidal fits (solid lines) yield a peak-to-peak signal amplitude A in the two detection bases $\langle\sigma_z\rangle$ (blue curve) and $\langle\sigma_y\rangle$ (red curve). To ensure maximum contrast for the cat state size used, the data is taken at light intensities that ensure a single photon scattering probability of $p = 1$. **b)** Line profile of the transition taken in the $\langle\sigma_y\rangle$ detection basis. At each spectroscopy laser frequency the signal difference between the oscillation's minimum and maximum is measured. To avoid power broadening the light level was reduced significantly, yielding a smaller signal due to $p \ll 1$.

TABLE I: **Comparison of spectroscopic techniques.** The sensitivity of various cat state spectroscopy (CSS) techniques, and those which do not employ a non-classical state, are compared (see text). Also given are the number of measurements required to reach a confidence of three standard deviations (σ) in detection of a scattering event. The ** indicate the result for a CSS measurement *without* ground state cooling. The errors are calculated from quantum projection noise.

Method	Sensitivity (β)	Measurements to reach 3σ
Direct detection $\langle\sigma_z\rangle$	0.018(6)	$2.7(1.9)\times10^{5}$
Phase-sensitive $\langle\sigma_y\rangle$ direct detection	0.107(10)	$7.8(1.5)\times10^{2}$
CSS $\langle\sigma_z\rangle$-signal	0.162(16)	$3.4(0.6)\times10^{2}$
CSS $\langle\sigma_y\rangle$-signal	0.338(16)	$7.9(0.8)\times10^{1}$
CSS $\langle\sigma_y\rangle$-signal**	0.109(14)	$7.6(2.0)\times10^{2}$

Supplementary online material

Random geometric phases by electric field noise causing motional heating

Motional heating during the cat state generation, photon scattering and cat state recombination gives rise to additional geometric phases that reduce the contrast of the signal. In this online material we show that due to heating, a random phase Φ_h is produced during cat state creation and recombination which is given by

$$\langle \Phi_h^2 \rangle = \frac{16}{3} n_{cat} R_h \tau \tag{2}$$

where $n_{\rm cat} = |\alpha|^2$ is the size of the cat state in terms of its average phonon number, R_h the motional heating rate, and τ the length of the two time intervals in which the cat state is created and and subsequently put back again into the initial state.

To model the heating, we divide the time interval $T = 2\tau$ into N small intervals of length $dt = T/N$ and follow the time evolution of one of the motional components of the cat state. In each of these intervals, fluctuating electric fields will displace the motional state by an amount $d\beta_i = dx_i + dp_i$ where the projections of $d\beta_i$ onto the x- and the p-axis are normally distributed independent random variables with variance $\sigma^2 = \frac{1}{2} R_h dt$. This can be seen by noting that, after time T, the motional state displacement due to heating alone is given by

$$\beta(T) = \sum_{i=1}^{N} d\beta_i = \sum_{i=1}^{N} dx_i + dp_i$$

and the average vibrational quantum number becomes

$$\langle |\beta(T)|^2 \rangle = \sum_{i}^{N} (\langle dx_i^2 \rangle + \langle dp_i^2 \rangle) = R_h dt N = R_h T$$

in agreement with the definition of the heating rate.

In a first step, we will study the effect of motional heating on states that are coherently displaced in phase space by some classical well-controlled driving force. In the absence of motional heating, we assume that the initial state $|0\rangle$ is coherently displaced with a (arbitrary) trajectory described by $|\alpha(t)\rangle$. We are interested in the case where the (transient) motional excitation by the coherent drive is much bigger than the excitation by the random fluctuating force causing motional heating. We now look at the effect of a heating event (an undesired kick of the motional state) at time t_i on the state. Before this event, the state was coherently displaced by an amount $\alpha_1 = \alpha(t_i) - \alpha(t = 0)$ where $\alpha(t = 0) = 0$. After the event, the coherent displacement is given by $\alpha_2 = \alpha(T) - \alpha(t_i)$. The heating event itself displaces the state by an amount $d\beta_i$. In the absence of heating, the final state at time T is given by

$$|\alpha(T)\rangle = D(\alpha(T))|0\rangle = e^{-iIm(\alpha_1^* \alpha_2)} D(\alpha_2) D(\alpha_1) |0\rangle$$

where the phase factor cancels the phase arising from the multiplication of the two displacement operations. In the presence of heating at time t_i, the state is modified to

$$\begin{aligned} |\psi\rangle &= e^{-iIm(\alpha_1^* \alpha_2)} D(\alpha_2) D(d\beta_i) D(\alpha_1) |0\rangle \\ &= e^{iIm(\alpha_1^* d\beta_i + d\beta_i^* \alpha_2)} D(\alpha_2 + d\beta_i + \alpha_1) |0\rangle \\ &= e^{iIm(\alpha_1^* d\beta_i + d\beta_i^* \alpha_2)} |\alpha(T) + d\beta_i\rangle, \end{aligned} \tag{3}$$

i.e., the state experiences a small additional displacement and is multiplied by the heating-induced random phase

$$\begin{aligned} \phi_i &= Im(\alpha_1^* \, d\beta_i + d\beta_i^* \, \alpha_2) \\ &= Im(\alpha_1^* \, d\beta_i) + Im(d\beta_i^* \, \alpha_2) \\ &= Im(\alpha_1^* \, d\beta_i) - Im(d\beta_i \, \alpha_2^*) \\ &= Im((\alpha_1 - \alpha_2)^* \, d\beta_i). \end{aligned} \tag{4}$$

If the coherent displacement $\alpha(t)$ is much bigger than the heating-induced displacement, the final state is to a good approximation equal to $|\alpha(T)\rangle$ multiplied by the product of all heating-induced phase factors occuring in the interval $[0, T]$. Equation (4) can be further simplified by splitting $d\beta_i$ into two random variables du_i (dv_i) that are oriented orthogonal (parallel) to $(\alpha_1 - \alpha_2)^*$ and each have variances σ^2 so that

$$\phi_i = |\alpha_1 - \alpha_2| du_i \sin\theta_i$$

where $\theta_i = \pm \pi/2$ is the angle between the orthogonal component of $d\beta_i$ and $(\alpha_1 - \alpha_2)^*$. This term ensures that trajectories $|\alpha(t)\rangle$ in opposite directions pick up opposite geometric phases: as in the case of the two motional components in the generation/recombination of the cat state.

After simple substitution, the heating-induced geometric phase acquired by the coherent state $\alpha(T)$ is given by

$$\Phi_g = \sum_{i=1}^{N} \phi_i = \sum_{i} |2\alpha(t_i) - \alpha(T_N) - \alpha(0)| du_i \sin\theta_i$$

which reduces to

$$\Phi_g = 2 \sum_{i} |\alpha(t_i)| du_i \sin\theta_i \tag{5}$$

in the case $\alpha(T_N) = \alpha(0) = 0$.

For a cat state that is created and recombined, both components acquire heating-induced phases $\pm\Phi_g$ of opposite sign. Therefore, the relative phase between the two components is $\Phi_h = 2\Phi_g$. We can calculate its mean-squared value:

$$\langle \Phi_h^2 \rangle = 16 \sum_{k=1}^{N} |\alpha(t_k)|^2 \langle du_i^2 \rangle = 8R_h \sum_{k=1}^{N} |\alpha(t_k)|^2 \, dt = 8R_h \int_0^T |\alpha(t)|^2 \, dt. \quad (6)$$

For

$$\alpha(t) = \begin{cases} \sqrt{n_{cat}}\, t/\tau & : \ t \le \tau \\ \sqrt{n_{cat}}\, (2\tau - t)/\tau & : \ \tau \le t \le 2\tau \end{cases}$$

the mean squared phase is given by

$$\langle \Phi_h^2 \rangle = \frac{16}{3} R_h \tau n_{cat} \quad (7)$$

which is the result stated at the beginning in eq. (2). It is easy to include an additional waiting time t_{wait} between cat creation and recombination in the calculation. For

$$\alpha(t) = \begin{cases} \sqrt{n_{cat}}\, t/\tau & : \ t \le \tau \\ \sqrt{n_{cat}} & : \ \tau \le t \le \tau + t_{wait} \\ \sqrt{n_{cat}}\, (2\tau + t_{wait} - t)/\tau & : \ \tau + t_{wait} \le t \le 2\tau + t_{wait} \end{cases}$$

integration of eq. (6) yields the mean-squared phase

$$\langle \Phi_h^2 \rangle = 8R_h n_{cat} (\frac{2\tau}{3} + t_{wait}). \quad (8)$$

For a random variable X that has a Gaussian distribution with $\langle X \rangle = 0$, the equality

$$\langle \cos X \rangle = \exp(-\frac{\langle X^2 \rangle}{2})$$

holds which enables us to calculate the loss of Ramsey contrast of the cat state spectroscopy from eqs.(7) or (8).